

# Multicomponent fluid of nonadditive hard spheres near a wall

Riccardo Fantoni\*

*Dipartimento di Scienze dei Materiali e Nanosistemi, Università Ca' Foscari Venezia,  
Calle Larga S. Marta DD2137, I-30123 Venezia, Italy*

Andrés Santos†

*Departamento de Física, Universidad de Extremadura, E-06071 Badajoz, Spain*

(Dated: April 8, 2013)

A recently proposed rational-function approximation [Phys. Rev. E **84**, 041201 (2011)] for the structural properties of nonadditive hard spheres is applied to evaluate analytically (in Laplace space) the local density profiles of multicomponent nonadditive hard-sphere mixtures near a planar nonadditive hard wall. The theory is assessed by comparison with *NVT* Monte Carlo simulations of binary mixtures with a size ratio 1:3 in three possible scenarios: a mixture with either positive or negative nonadditivity near an additive wall, an additive mixture with a nonadditive wall, and a nonadditive mixture with a nonadditive wall. It is observed that, while the theory tends to underestimate the local densities at contact (especially in the case of the big spheres) it captures very well the initial decay of the densities with increasing separation from the wall and the subsequent oscillations.

PACS numbers: 61.20.Gy, 61.20.Ne, 61.20.Ja, 68.08.De

## I. INTRODUCTION

The study of mixtures near a fluid-solid interface is important for the understanding of wetting and adsorption phenomena where competition among different components may occur. A simplified physical picture of adsorption may be obtained at a microscopic level if one considers the solid surface as a planar smooth hard wall confining the particles of the mixture. Thereby, one can describe the expected oscillations of the (partial) local particle densities in the neighborhood of the wall with an abundance of particles right at contact and a depletion nearby. Whereas confined fluid mixtures of additive hard spheres (AHS) have been widely studied within integral equation theories [1–8], Monte Carlo simulations [8–13], and density-functional theories [9, 13–23], much less is known in the case of nonadditive hard spheres (NAHS) [24–27].

In a recent paper [28], NAHS mixtures were studied through the so-called rational-function approximation (RFA) technique [29, 30], which amounts to choosing simple (rational-function) expressions for the Laplace space representation of the radial distribution functions of the theory of liquids [31, 32]. This allowed us to determine a nonperturbative, fully analytical (in Laplace space) approximation. When the nonadditivity is set to zero, the approximation reduces to the Percus–Yevick (PY) approximation for an AHS mixture.

The purpose of the present work is to use the RFA scheme devised in Ref. [28] to determine the structural properties of an  $n$ -component NAHS fluid near a hard wall interacting either additively or nonadditively with

the particles of the fluid mixture. A realization of the problem is obtained from a  $(n + 1)$ -component NAHS mixture, where one of the species, species 0, is taken to have a vanishing concentration and an infinite diameter. A similar approach was employed by Malijevsky *et al.* [13] to determine through the RFA the structural properties of a multicomponent AHS fluid near an additive hard wall. In the present case, however, not only the particle-particle interaction may be nonadditive (i.e., the closest distance between the centers of two spheres of species  $i$  and  $j$  is in general different from the arithmetic mean of the respective diameters), but also the particle-wall may be nonadditive as well. The latter possibility means that the closest distance from the planar wall to the center of a sphere may be different from the radius of the sphere. A similar problem has recently been considered by González *et al.* [33], where strong size selectivity is observed in a binary AHS mixture confined in a narrow cylindrical pore such that each species of the mixture sees a different cylinder radius.

We will compare our approximation results for the local density of particles at a distance  $z$  from the wall with exact canonical (fixed number of particles  $N$ , volume  $V$ , and temperature  $T$ ) Monte Carlo (MC) simulation results for binary mixtures. In the simulation it is necessary to use two hard walls on the opposite far square faces of a parallelepiped simulation box with rectangular lateral faces and to choose the two walls far enough so that bulk properties of the fluid can be extracted by looking at the center of the box.

The agreement between theory and simulations is quite satisfactory. It is worse at contact (similarly to what happens with the PY theory in the additive case [13]) but it rapidly improves as the distance from the wall increases, so that the first minimum (depletion region) and the subsequent oscillations are well predicted by our analytical

\* rfantoni@ts.infn.it

† andres@unex.es; <http://www.unex.es/eweb/fisteor/andres>

approach. To the best of our knowledge, our results constitute the first proposal for an analytical expression (in Laplace space) for the density profiles of a NAHS mixture confined by a (nonadditive or additive) hard wall. As such, the theory is expected to be useful to the experimentalist who needs easy formulas to determine profiles to compare with experimental data, thus bypassing the need of numerical experiments.

The paper is organized as follows. In Sec. II we describe the model of the confined fluid we are going to study. The RFA used to extract the structural properties of the fluid is presented in Sec. III, where some details of the wall limit are given in the Appendix. In Sec. IV we describe some details of the  $NVT$  MC simulation method we employed for confined binary mixtures. The results for the structural properties are presented in Sec. V, where the RFA and our own MC simulation are compared. Finally, Sec. VI is left for concluding remarks.

## II. THE MODEL

An  $n$ -component NAHS mixture in the  $d$ -dimensional Euclidean space is a fluid of  $N_i$  particles of species  $i$  with  $i = 1, 2, \dots, n$ , such that there are a total number of particles  $N = \sum_{i=1}^n N_i$  in a volume  $V$ , and the pair potential between a particle of species  $i$  and a particle of species  $j$  separated by a distance  $r$  is given by

$$\phi_{ij}(r) = \begin{cases} \infty, & r \leq \sigma_{ij}, \\ 0, & r > \sigma_{ij}, \end{cases} \quad (2.1)$$

where  $\sigma_{ii} = \sigma_i$  and  $\sigma_{ij} = \frac{1}{2}(\sigma_i + \sigma_j)(1 + \Delta_{ij})$ , so that  $\Delta_{ii} = 0$  and  $\Delta_{ij} = \Delta_{ji} > -1$ . When  $\Delta_{ij} = 0$  for every pair  $i$ - $j$  we recover the AHS system. In the present paper we will only consider the NAHS system in its single fluid phase.

Let  $\bar{\rho} = N/V$  be the total number density of the mixture and  $\bar{x}_i = N_i/N$  be the mole fraction of species  $i$ . These are spatially averaged quantities that can differ from local values in confined situations.

The one-dimensional ( $d = 1$ ) NAHS fluid admits an exact analytical solution for the structural and thermophysical properties in the thermodynamic limit  $N \rightarrow \infty$  with  $\bar{\rho} = N/V = \text{const}$  [34–37]. Moreover, the AHS fluid with  $d = \text{odd}$  allows for an analytical solution of the PY approximate theory [38–41]. Such a solution in the case  $d = 1$  reduces to the exact solution particularized to the additive mixture.

Inspired by both the exact solution for one-dimensional NAHS mixtures and the PY solution for three-dimensional AHS mixtures, we have recently proposed an analytical approach for the three-dimensional NAHS system [28]. As said in Sec. I, the aim of the present paper is to use that approximation to determine the structural properties of a ternary mixture where one of the species ( $i = 0$ ) is subject to the *wall limit*:  $\bar{x}_0 \rightarrow 0$  and  $\sigma_0 \rightarrow \infty$ . Such a ternary mixture represents a binary mixture of

AHS ( $\Delta_{12} = 0$ ) or NAHS ( $\Delta_{12} \neq 0$ ) in the presence of a hard wall which, in addition, may interact additively or nonadditively with the fluid particles (see Sec. III B).

## III. RATIONAL-FUNCTION APPROXIMATION

### A. General scheme

In Ref. [28], the following proposal for the structural properties of an  $n$ -component NAHS fluid defined through the Laplace transform  $G_{ij}(s)$  of  $rg_{ij}(r)$  was given:

$$G_{ij}(s) = s^{-2} \sum_{k=1}^n e^{-\sigma_{ik}s} L_{ik}(s) B_{kj}(s), \quad (3.1)$$

with

$$B^{-1}(s) = \mathbf{l} - \mathbf{A}(s), \quad (3.2)$$

$$A_{ij}(s) = \frac{2\pi\bar{\rho}\bar{x}_i}{s^3} [N_{ij}(s)e^{a_{ij}s} - L_{ij}(s)e^{-\sigma_{ij}s}], \quad (3.3)$$

where  $\mathbf{l}$  is the unit matrix,

$$L_{ij}(s) \equiv L_{ij}^{(0)} + L_{ij}^{(1)} s, \quad (3.4)$$

$$N_{ij}(s) \equiv L_{ij}^{(0)} \left( 1 - b_{ij}s + \frac{b_{ij}^2 s^2}{2} \right) + L_{ij}^{(1)} s (1 - b_{ij}s), \quad (3.5)$$

$$b_{ij} \equiv \sigma_{ij} + a_{ij}, \quad a_{ij} \equiv \frac{1}{2}(\sigma_i - \sigma_j). \quad (3.6)$$

Equations (3.1)–(3.5) provide the explicit  $s$ -dependence of the Laplace transform  $G_{ij}(s)$ , but it still remains to obtain the two sets of parameters  $L_{ij}^{(0)}$  and  $L_{ij}^{(1)}$ . This is done by enforcing the physical requirements  $\lim_{s \rightarrow 0} s^2 G_{ij}(s) = 1$  and  $\lim_{s \rightarrow 0} s^{-1} [s^2 G_{ij}(s) - 1] = 0$  [28]. The result is

$$L_{ij}^{(0)} = S_j, \quad L_{ij}^{(1)} = T_j + \sigma_{ij} S_j, \quad (3.7)$$

where

$$S_j \equiv \frac{1 - \pi\bar{\rho}\Psi_j}{(1 - \pi\bar{\rho}\Lambda_j)(1 - \pi\bar{\rho}\Psi_j) - \pi^2\bar{\rho}^2\mu_{j|2,0}\Omega_j}, \quad (3.8)$$

$$T_j \equiv \frac{\pi\bar{\rho}\Omega_j}{(1 - \pi\bar{\rho}\Lambda_j)(1 - \pi\bar{\rho}\Psi_j) - \pi^2\bar{\rho}^2\mu_{j|2,0}\Omega_j}, \quad (3.9)$$

$$\Lambda_j \equiv \mu_{j|2,1} - \frac{1}{3}\mu_{j|3,0}, \quad (3.10)$$

$$\Psi_j \equiv \frac{2}{3}\mu_{j|3,0} - \mu_{j|2,1}, \quad (3.11)$$

$$\Omega_j \equiv \mu_{j|3,1} - \mu_{j|2,2} - \frac{1}{4}\mu_{j|4,0}, \quad (3.12)$$

and we have called

$$\mu_{j|p,q} \equiv \sum_{k=1}^n \bar{x}_k b_{kj}^p \sigma_{kj}^q. \quad (3.13)$$

As discussed in Ref. [28], the inverse Laplace transform  $\mathcal{L}^{-1}[G_{ij}(s)](r)$  may present a spurious behavior in the shell  $\min(\sigma_{ij}, \tau_{ij}) \leq r \leq \max(\sigma_{ij}, \tau_{ij})$ , where  $\tau_{ij}$  is the minimum of the list of values  $\sigma_{ik} - a_{kj}$  ( $k = 1, \dots, n$ ) that are different from  $\sigma_{ij}$ . If  $\sigma_{ik} - a_{kj} = \sigma_{ij}$  for all  $k$ , then  $\tau_{ij} = \sigma_{ij}$ . The anomalous behavior of  $\mathcal{L}^{-1}[G_{ij}(s)](r)$  for  $\min(\sigma_{ij}, \tau_{ij}) \leq r \leq \max(\sigma_{ij}, \tau_{ij})$  can be avoided with a series of corrections, the simplest one of which yields

$$g_{ij}(r) = \Theta(r - \sigma_{ij}) \left[ \frac{\mathcal{L}^{-1}[G_{ij}(s)](r)}{r} + C_{ij} \Theta(\tau_{ij} - r) \left( \frac{\tau_{ij}}{r} - 1 \right) \right], \quad (3.14)$$

where

$$C_{ij} = 2\pi \bar{\rho} \bar{x}_{\kappa_{ij}} L_{i\kappa_{ij}}^{(1)} \left( L_{\kappa_{ij}j}^{(1)} - S_j \frac{b_{\kappa_{ij}j}}{2} \right) b_{\kappa_{ij}j}, \quad (3.15)$$

$\kappa_{ij}$  being the index associated with  $\tau_{ij}$ ; i.e.,  $\tau_{ij} = \sigma_{i\kappa_{ij}} - a_{\kappa_{ij}j}$ . The contact values are given by [28]

$$g_{ij}(\sigma_{ij}^+) = \frac{L_{ij}^{(1)}}{\sigma_{ij}} + C_{ij} \left( \frac{\tau_{ij}}{\sigma_{ij}} - 1 \right). \quad (3.16)$$

The approximation (3.14) was referred to as RFA<sub>+</sub><sup>(1)</sup> in Ref. [28]. In the special case of AHS mixtures, one has  $\sigma_{ik} - a_{kj} = \sigma_{ij}$ , so that  $\tau_{ij} = \sigma_{ij}$  and  $g_{ij}(r) = r^{-1} \mathcal{L}^{-1}[G_{ij}(s)](r)$  coincides with the PY solution [38, 39].

## B. Wall limit

Now we assume that a single sphere of diameter  $\sigma_0$  is introduced in the  $n$ -component fluid. This gives rise to an  $(n+1)$ -component fluid, where the extra species ( $i=0$ ), being made of a single particle, has a vanishing concentration  $\bar{x}_0 = 0$  in the thermodynamic limit  $N \rightarrow \infty$ . With this proviso, Eq. (3.1) can be easily extended to this  $(n+1)$ -component mixture.

According to Eq. (3.3), if  $\bar{x}_0 = 0$ , the row  $i=0$  of the matrix  $\mathbf{A}$  is zero. As a consequence, the row  $i=0$  and the column  $j=0$  of the matrices  $\mathbf{B}^{-1}$  and  $\mathbf{B}$  have the forms

$$B_{0j}^{-1} = \delta_{j0}, \quad B_{i0}^{-1} = -A_{i0}, \quad i \geq 1, \quad (3.17)$$

$$B_{0j} = \delta_{j0}, \quad B_{i0} = \sum_{k=1}^n B_{ik} A_{k0}, \quad i \geq 1. \quad (3.18)$$

Thus, application of Eq. (3.1) to the pair  $i-0$  with  $i \geq 1$  yields

$$G_{i0}(s) = s^{-2} e^{-\sigma_{i0}s} L_{i0}(s) + \sum_{j=1}^n G_{ij}(s) A_{j0}(s). \quad (3.19)$$

Therefore, the cross function  $G_{i0}(s)$  (with  $i = 1, \dots, n$ ), which is related to the spatial correlation between a particle of species  $i \geq 1$  and the single particle  $i=0$ , is expressed in terms of the matrix  $G_{ij}(s)$  of the  $n$ -component mixture and the cross elements  $L_{i0}(s)$  and  $A_{j0}(s)$ .

In principle, the nonadditivity of the  $i-0$  interaction would be measured by the nonadditivity parameter  $\Delta_{i0}$  defined by  $\sigma_{i0} = \frac{1}{2}(\sigma_0 + \sigma_i)(1 + \Delta_{i0})$ . However, the use of  $\Delta_{i0}$  is not convenient in the wall limit  $\sigma_0 \rightarrow \infty$  that we will take at the end. Instead, we define a nonadditivity distance  $w_i$  by  $\sigma_{i0} = \frac{1}{2}(\sigma_0 + \sigma_i) + w_i$ . Note that, since no 0-0 interaction is present, the definition of the diameter  $\sigma_0$  is somewhat arbitrary. In fact, if all  $w_i = w$  are equal, the apparently nonadditive  $i-0$  interaction is indistinguishable from an additive interaction with  $\sigma_0 \rightarrow \sigma_0 + 2w$ . Therefore, a true nonadditive  $i-0$  interaction requires, first, that  $n \geq 2$  and, second, that not all  $\{w_i\}$  are equal. Therefore, without loss of generality, we take  $\min(w_i; i = 1, \dots, n) = 0$ . This defines the diameter  $\sigma_0$  unambiguously.

As a next step toward the wall limit, we introduce the shifted radial distribution function

$$\gamma_i(z) = g_{i0}(z + \sigma_0/2). \quad (3.20)$$

Thus, while  $r$  is the distance between the centers of the pair  $i-0$ ,  $z = r - \frac{1}{2}\sigma_0$  represents the distance from the center of a sphere of species  $i$  to the surface of the single sphere  $j=0$ . If we call  $\Gamma_i(s)$  the Laplace transform of  $\gamma_i(z)$ , the following relationship applies:

$$G_{i0}(s) = e^{-\sigma_0 s/2} \left[ \frac{\sigma_0}{2} \Gamma_i(s) - \Gamma_i'(s) \right], \quad (3.21)$$

where  $\Gamma_i'(s) = \partial \Gamma_i(s) / \partial s$ .

Finally, we take the wall limit  $\sigma_0 \rightarrow \infty$ . In that case, the function  $\gamma_i(z)$  becomes the ratio between the local number density of particles of species  $i$  at a distance  $z$  from the wall,  $\rho_i(z)$ , and the corresponding density in the bulk,  $\rho_i^b$ . In an infinite system (as implicitly assumed in the theoretical approach), the bulk and average values coincide, i.e.,  $\rho_i^b = \rho_i(\infty) = \bar{x}_i \bar{\rho}$ .

In the wall limit  $\Gamma_i'(s)$  can be neglected versus  $\sigma_0 \Gamma_i(s)/2$  in Eq. (3.21), so that

$$\begin{aligned} \Gamma_i(s) &= 2 \lim_{\sigma_0 \rightarrow \infty} \sigma_0^{-1} e^{\sigma_0 s/2} G_{i0}(s) \\ &= 2 e^{-(\sigma_i/2 + w_i)s} \frac{\tilde{L}_i(s)}{s^2} + 2 \sum_{j=1}^n G_{ij}(s) \tilde{A}_j(s), \end{aligned} \quad (3.22)$$

where in the second step we have made use of Eq. (3.19) and have defined

$$\tilde{L}_i(s) \equiv \lim_{\sigma_0 \rightarrow \infty} \sigma_0^{-1} L_{i0}(s), \quad (3.23)$$

$$\tilde{A}_j(s) \equiv \lim_{\sigma_0 \rightarrow \infty} \sigma_0^{-1} e^{\sigma_0 s/2} A_{j0}(s). \quad (3.24)$$

These two quantities are evaluated in the Appendix.

Once the Laplace transform  $\Gamma_i(s)$  is well defined, let us consider the correction described by the second line of Eq. (3.14). First, we subtract  $\frac{1}{2}\sigma_0$  to the distances, so that the shell  $\min(\sigma_{i0}, \tau_{i0}) \leq r \leq \max(\sigma_{i0}, \tau_{i0})$  becomes  $\min(\frac{1}{2}\sigma_i + w_i, \tilde{\tau}_i) \leq z \leq \max(\frac{1}{2}\sigma_i + w_i, \tilde{\tau}_i)$ , where  $\tilde{\tau}_i$  is the minimum of the list of values  $\sigma_{ik} - \frac{1}{2}\sigma_k$  ( $k = 1, \dots, n$ ) that differ from  $\frac{1}{2}\sigma_i + w_i$ . Again,  $\tilde{\tau}_i = \frac{1}{2}\sigma_i + w_i$  if  $\sigma_{ik} - \frac{1}{2}\sigma_k = \frac{1}{2}\sigma_i + w_i$  for all  $k$ . Finally, in the limit  $\sigma_0 \rightarrow \infty$ , one obtains

$$\gamma_i(z) = \Theta\left(z - \frac{1}{2}\sigma_i - w_i\right) \left[ \mathcal{L}^{-1}\{\Gamma_i(s)\}(r) + 2\tilde{C}_i \Theta(\tilde{\tau}_i - z) (\tilde{\tau}_i - z) \right], \quad (3.25)$$

with

$$\tilde{C}_i = 2\pi \bar{\rho} \bar{x}_{\kappa_i} L_{i\kappa_i}^{(1)} \left( \tilde{L}_{\kappa_i}^{(1)} - \tilde{L}^{(0)} \frac{\sigma_{\kappa_i} + w_{\kappa_i}}{2} \right) (\sigma_{\kappa_i} + w_{\kappa_i}), \quad (3.26)$$

where  $\kappa_i$  is the index associated with  $\tilde{\tau}_i$ , i.e.,  $\tilde{\tau}_i = \sigma_{i\kappa_i} - \frac{1}{2}\sigma_{\kappa_i}$ , and the quantities  $\tilde{L}^{(0)}$  and  $\tilde{L}_i^{(1)}$  are defined in the Appendix.

The inverse Laplace transform in Eq. (3.25) can be easily performed numerically [42]. On the other hand, the density ratio  $\gamma_i$  at the shortest distance from the wall  $z = \frac{1}{2}\sigma_i + w_i$  can be derived analytically. From Eq. (3.16) we easily obtain

$$\gamma_i\left(z = \frac{1}{2}\sigma_i + w_i\right) = 2\tilde{L}_i^{(1)} + 2\tilde{C}_i \left( \tilde{\tau}_i - \frac{1}{2}\sigma_i - w_i \right). \quad (3.27)$$

The fact that the general scheme gives well defined expressions in the wall limit ( $\bar{x}_0 = 0, \sigma_0 \rightarrow \infty$ ) is a stringent test on the internal consistency of the RFA approach. It also shows the convenience of dealing with explicit, analytical expressions from which the subsequent limits can be taken.

#### IV. MONTE CARLO SIMULATIONS

We have simulated a binary mixture ( $n = 2$ ) of NAHS through canonical  $NVT$  MC simulations in a box of fixed volume and sides  $L_x, L_y$ , and  $L_z$  with  $L_x = L_y$  and  $L_z \gg L_x$ . Periodic boundary conditions are enforced along the  $x$  and  $y$  directions, but two impenetrable hard walls are located at  $z = 0$  and  $z = L_z$ . The particles are initially placed on a simple cubic regular configuration along the  $z$  direction with a first crystal layer of particles of species 1 juxtaposed to a crystal layer of particles of species 2. We reject the  $i$ th particle move only in case of overlap with any other particle, i.e., if  $r_{ij} < \sigma_{ij}$  for some  $j$ , or with one of the walls, i.e., if  $\min(z_i, L_z - z_i) < \frac{1}{2}\sigma_i + w_i$ . The system is then equilibrated for  $10^7$  MC steps (where a MC step corresponds

to a single particle move) and the properties are generally averaged over additional  $10^9$  MC steps for production. The maximum particle displacement, the same along each direction, is determined during the first stage of the equilibration run in such a way as to ensure an average acceptance ratio of 50% at production time. As a compromise between the condition  $L_z \gg L_x$  and the computational need of not having too high a number of particles, we have taken  $L_x = 10\sigma_1$  and  $L_z = 30\sigma_1$  in all the simulations presented, except a control case with  $L_z = 60\sigma_1$  (see below). The local density profiles  $\gamma_i(z) = \rho_i(z)/\rho_i^b$  are obtained, for each species, from histograms of the  $z$  coordinates of the particles in bins of width  $0.01\sigma_1$ . The bulk values  $\rho_i^b$  are evaluated in the region of the simulation box with  $z \approx L_z/2$ , where a negligible influence from the walls is expected. Due to the finite value of  $L_z$ , the bulk total density  $\rho^b = \rho_1^b + \rho_2^b$  and the bulk mole fraction  $x_1^b = \rho_1^b/\rho^b$  differ from their respective average values  $\bar{\rho}$  and  $\bar{x}_1$ .

## V. RESULTS

### A. Representative systems

In the binary case, there are five independent dimensionless parameters of the problem: the size ratio  $\sigma_2/\sigma_1$ , the particle-particle nonadditivity parameter  $\Delta_{12}$ , the particle-wall nonadditivity parameter  $\max(w_1, w_2)/\sigma_1$  [remember that, by convention,  $\min(w_1, w_2) = 0$ ], the average mole fraction  $\bar{x}_1$ , and the average reduced density  $\bar{\rho}\sigma_1^3$ . Here,  $\sigma_1$  is chosen as the diameter of the small spheres and henceforth it will be used to define the length unit.

In order to focus on the nonadditivity parameters, we have chosen  $\sigma_2/\sigma_1 = 3$  for all the systems. Next, three classes of systems have been considered: (i) a nonadditive mixture in the presence of an additive wall, (ii) an additive mixture in the presence of a nonadditive wall, and (iii) a nonadditive mixture with a nonadditive wall. As representative examples of class (i) we have chosen an equimolar mixture with either positive (system A of Table I) or negative (system B of Table I) nonadditivity and a mixture with an excess of small spheres and negative nonadditivity at two densities (systems C1 and C2, respectively). As examples of class (ii), we have chosen an equimolar mixture where the wall presents an extra repulsion to either the large spheres (system D) or the small spheres (system E). Finally, class (iii) is represented by system F, which is analogous to system D, except that the mixture has a negative nonadditivity. The reduced densities  $\bar{\rho}\sigma_1^3$  range from  $\frac{1}{30}$  to  $\frac{1}{5}$ , so that the total number of particles  $N = \bar{\rho}L_x^2L_z$  ranges from 100 to 600. It is also convenient to measure the density in terms of the *effective* packing fraction  $\bar{\eta}_{\text{eff}} = \frac{\pi}{6}\bar{\rho}\sum_{i,j}\bar{x}_i\bar{x}_j\sigma_{ij}^3$  related to van der Waals's one-fluid theory [43], whose values are indicated in the last column of Table I. In the low-density regime, two mixtures with the same value of  $\bar{\eta}_{\text{eff}}$  would

TABLE I. Values of the nonadditivity parameters ( $\Delta_{12}$ ,  $w_1$ , and  $w_2$ ), the average mole fraction ( $\bar{x}_1$ ), and the average density ( $\bar{\rho}$ ) for the representative systems considered in this work. In all the cases  $\sigma_2/\sigma_1 = 3$ . The table also includes the values ( $x_1^b$  and  $\rho^b$ ) measured in the bulk region  $z \approx L_z/2$  in our MC simulations with  $L_z/\sigma_1 = 30$ .

Label	$\Delta_{12}$	$w_1/\sigma_1$	$w_2/\sigma_1$	$\bar{x}_1$	$x_1^b$	$\bar{\rho}\sigma_1^3$	$\rho^b\sigma_1^3$	$\bar{\eta}_{\text{eff}}$
A	0.2	0	0	0.5	0.469	$\frac{1}{30}$	0.0337	0.243
B	-0.2	0	0	0.5	0.503	$\frac{1}{20}$	0.0513	0.237
C1	-0.2	0	0	0.9	0.896	$\frac{1}{10}$	0.1025	0.095
C2	-0.2	0	0	0.9	0.898	$\frac{1}{5}$	0.2040	0.190
D	0	0	0.35	0.5	0.475	$\frac{1}{30}$	0.0345	0.192
E	0	0.35	0	0.5	0.511	$\frac{1}{20}$	0.0503	0.288
F	-0.2	0	0.35	0.5	0.486	$\frac{1}{30}$	0.0350	0.158

have the same compressibility factor.

### B. Bulk values

The bulk values  $x_1^b$  and  $\rho^b$  measured in the MC simulations with  $L_z = 30\sigma_1$  are also included in Table I. In all the cases the bulk density  $\rho^b$  is larger than the average density  $\bar{\rho}$ . This is due to the fact that the effective length available to the spheres of species  $i$  is not  $L_z$  but  $L_z - (\sigma_i + 2w_i)$ . As a consequence, the larger deviation between  $\rho^b$  and  $\bar{\rho}$  takes place for systems D (3.5%) and F (5.0%), i.e., those systems where the walls produce an extra repulsion ( $w_2/\sigma_1 = 0.35$ ) on the big spheres. This compression effect is only partially compensated by the accumulation of particles at contact with the walls. In the case of the bulk mole fraction  $x_1^b$ , the situation is less obvious. Note the identity

$$\frac{\bar{x}_1\bar{\rho}}{x_1^b\rho^b} = \frac{1}{L_z/2} \int_{\sigma_1/2+w_1}^{L_z/2} dz \gamma_1(z). \quad (5.1)$$

Even if the right-hand side of Eq. (5.1) is generally smaller than 1, the fact that  $\rho^b > \bar{\rho}$  can give rise to  $x_1^b < \bar{x}_1$ ; i.e., the bulk would be richer in big spheres than on average. This is what actually happens for systems A, C1, C2, D, and F. This effect is especially important in systems A and D since in those cases the right-hand side of Eq. (5.1) turns out to be larger than 1 (see Figs. 1 and 5 below for a visual confirmation). Exceptions to the property  $x_1^b < \bar{x}_1$  are represented by systems B and E. In those cases, the right-hand side of Eq. (5.1) is sufficiently smaller than 1 (see Figs. 3 and 6 below) as to compensate for the ratio  $\rho^b/\bar{\rho} > 1$ .

Now we turn our attention to the density profiles. When presenting the theoretical RFA results for each system we have used two criteria. In the first criterion, the quantities  $\bar{\rho}$  and  $\bar{x}_1$  appearing in the theoretical scheme described in Sec. III have been identified with the average values employed in the simulations. In the second criterion, the RFA quantities  $\bar{\rho}$  and  $\bar{x}_1$  have been identified

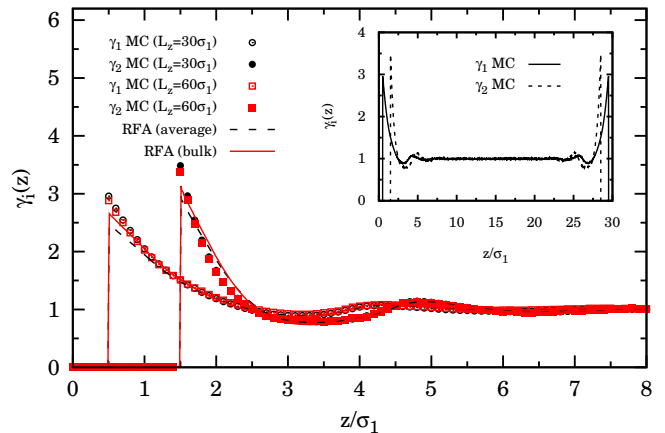


FIG. 1. (Color online) Local density profiles  $\gamma_i(z) = \rho_i(z)/\rho_i^b$  for system A ( $\sigma_2/\sigma_1 = 3$ ,  $\Delta_{12} = 0.2$ ,  $w_1 = w_2 = 0$ ,  $\bar{x}_1 = 0.5$ ,  $\bar{\rho}\sigma_1^3 = 1/30$ ). The lines represent the RFA theoretical predictions using the average values  $\bar{x}_1$  and  $\bar{\rho}$  (dashed lines) or the empirical bulk values  $x_1^b$  and  $\rho^b$  (solid lines). The symbols represent our MC simulations with  $L_z/\sigma_1 = 30$  (circles) or  $L_z/\sigma_1 = 60$  (squares). The inset shows the MC data in the whole domain  $0 < z < L_z$  with  $L_z/\sigma_1 = 30$ . In the MC results, the error bars are within the size of the symbols used in the graph.

with the bulk values  $\rho^b$  and  $x_1^b$  found in the MC simulations with  $L_z = 30\sigma_1$ . As said before, the theoretical approach deals with formally infinite systems ( $L_z \rightarrow \infty$ ) where the average and bulk quantities coincide. However, when making contact with simulation data corresponding to finite  $L_z$  the use of either the average or the bulk values in the RFA may be important.

### C. Nonadditive mixture and additive wall

Figure 1 shows the MC and RFA results for the two (relative) density profiles  $\gamma_i(z) = \rho_i(z)/\rho_i^b$  ( $i = 1, 2$ ) in the case of system A (positive nonadditivity). In this system  $\tilde{\tau}_1 = 0.9\sigma_1 > \frac{1}{2}\sigma_1$  and  $\tilde{\tau}_2 = 1.9\sigma_1 > \frac{1}{2}\sigma_2$ , so that the correction term given by the second line of Eq. (3.25) is used in the RFA curves.

The inset of Fig. 1 shows the MC results for both density profiles in the whole region  $0 < z < L_z = 30\sigma_1$ . We can see that the separation between both hard walls is large enough as to identify a well defined bulk region in the center. We have chosen system A to assess the influence of finite  $L_z$  by carrying out a control simulation with  $L_z = 60\sigma_1$ . The new bulk values are  $x_1^b = 0.485$  and  $\rho^b\sigma_1^3 = 0.0334$ , which, as expected, are closer to the average values than in the case  $L_z = 30\sigma_1$  (see Table I). As seen from Fig. 1, the MC data obtained with  $L_z = 30\sigma_1$  and  $L_z = 60\sigma_1$  are hardly distinguishable, except near contact where the smaller system, having a larger bulk

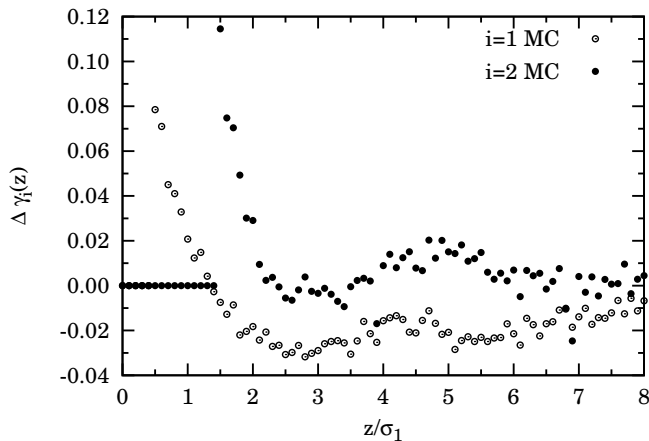


FIG. 2. Differences  $\Delta\gamma_i(z) = \gamma_i(z)|_{30} - \gamma_i(z)|_{60}$  between the local densities  $\gamma_i(z) = \rho_i(z)/\rho_i^b$  evaluated in MC simulations with  $L_z/\sigma_1 = 30$  and those evaluated in MC simulations with  $L_z/\sigma_1 = 60$  for system A ( $\sigma_2/\sigma_1 = 3$ ,  $\Delta_{12} = 0.2$ ,  $w_1 = w_2 = 0$ ,  $\bar{x}_1 = 0.5$ ,  $\bar{\rho}\sigma_1^3 = 1/30$ ).

density, presents slightly higher values of  $\gamma_i(z)$ . A more detailed comparison is made in Fig. 2, where the differences between the values of  $\gamma_i(z)$  as obtained with both values of  $L_z$  are shown. Figure 2 confirms that the smaller system ( $L_z = 30\sigma_1$ ) presents larger values for the two reduced densities near contact than the larger system ( $L_z = 60\sigma_1$ ). For higher separations the differences are much less important, but yet it is interesting to note that the smaller system tends to present larger values of  $\gamma_2(z)$  but smaller values of  $\gamma_1(z)$ .

Now let us go back to Fig. 1 and comment on the performance of the RFA. We observe that the RFA underestimates the local densities at contact (i.e., at  $z = \frac{1}{2}\sigma_i$ ). On the other hand, the decay of the local densities near the walls and the subsequent oscillations are very well captured by the theory. It is interesting to remark that the agreement with the MC data near contact improves when the bulk values instead of the average ones are used in the theory.

The profiles for system B (negative nonadditivity) are displayed in Fig. 3. In this case  $\tilde{\tau}_1 = 0.1\sigma_1$  and  $\tilde{\tau}_2 = 1.1\sigma_1$ . Since  $\tilde{\tau}_i < \frac{1}{2}\sigma_i$ , the correction term in the second line of Eq. (3.25) vanishes. Comparison between Figs. 1 and 3 shows that, in going from system A to system B, the local variation of the density of the big spheres is enhanced, while the local density of the small spheres becomes less structured. Here there are two competing effects at play. On the one hand, at a fixed density, the change from positive to negative nonadditivity produces a weaker density structure near the wall, as the exact result to first order in density clearly shows. On the other hand, at a fixed nonadditivity, an increase in density induces a higher structure. It seems that, in the transition from system A to system B, the latter effect dominates

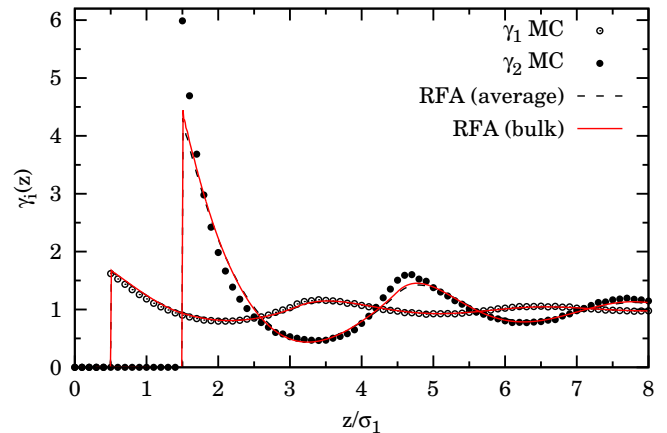


FIG. 3. (Color online) Local density profiles  $\gamma_i(z) = \rho_i(z)/\rho_i^b$  for system B ( $\sigma_2/\sigma_1 = 3$ ,  $\Delta_{12} = -0.2$ ,  $w_1 = w_2 = 0$ ,  $\bar{x}_1 = 0.5$ ,  $\bar{\rho}\sigma_1^3 = 1/20$ ). The lines represent the RFA theoretical predictions using the average values  $\bar{x}_1$  and  $\bar{\rho}$  (dashed lines) or the empirical bulk values  $x_1^b$  and  $\rho^b$  (solid lines). The symbols represent our MC simulations with  $L_z/\sigma_1 = 30$ . In the MC results, the error bars are within the size of the symbols used in the graph.

in the case of the big spheres (which are very weakly influenced by the small component) and the former effect does it in the case of the small spheres (which are strongly influenced by the presence of the large component). It is interesting to note that all these features are very well described by the RFA, especially in the case of  $\gamma_1(z)$ . The contact value of  $\gamma_2$  is better estimated in system A than in system B, while the opposite happens for the contact value of  $\gamma_1$ . Note also that a small discrepancy is observed near the second peak of  $\gamma_2(z)$  in Fig. 3. For this system the RFA is practically insensitive to the use of the bulk values instead of the average ones.

In systems A and B the big spheres occupy as much as 27 times more volume than the small ones, so the global properties of the mixture are dominated by species 2. A more balanced situation takes place in systems C1 and C2, where the ratio of partial packing fractions is  $\bar{x}_2\sigma_2^3/\bar{x}_1\sigma_1^3 = 3$ . In these cases the high concentration asymmetry requires a long simulation run time to reach thermal equilibrium for the big spheres.

The results for systems C1 and C2 are shown in Fig. 4. At the smaller density (system C1) the agreement between theory and simulation is almost perfect. As the density is doubled (system C2), some small deviations are visible, especially in the case of the big spheres. Again, the RFA with the bulk values behaves near contact better than with the average values.

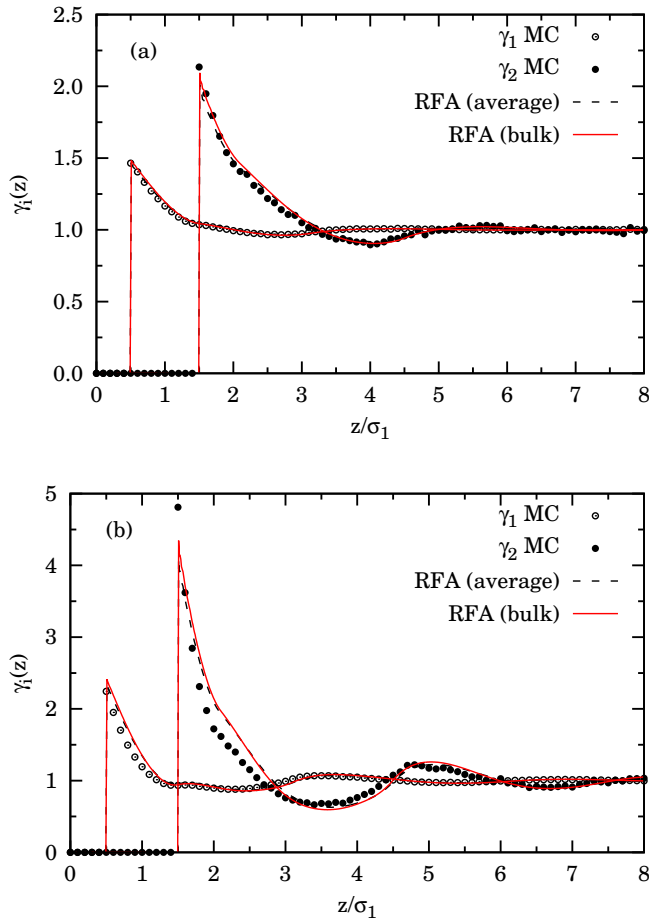


FIG. 4. (Color online) Local density profiles  $\gamma_i(z) = \rho_i(z)/\rho_i^b$  for (a) system C1 ( $\sigma_2/\sigma_1 = 3$ ,  $\Delta_{12} = -0.2$ ,  $w_1 = w_2 = 0$ ,  $\bar{x}_1 = 0.9$ ,  $\bar{\rho}\sigma_1^3 = 1/10$ ) and (b) system C2 ( $\sigma_2/\sigma_1 = 3$ ,  $\Delta_{12} = -0.2$ ,  $w_1 = w_2 = 0$ ,  $\bar{x}_1 = 0.9$ ,  $\bar{\rho}\sigma_1^3 = 1/5$ ). The lines represent the RFA theoretical predictions using the average values  $\bar{x}_1$  and  $\bar{\rho}$  (dashed lines) or the empirical bulk values  $x_1^b$  and  $\rho^b$  (solid lines). The symbols represent our MC simulations with  $L_z/\sigma_1 = 30$ . In the MC results, the error bars are within the size of the symbols used in the graph.

#### D. Additive mixture and nonadditive wall

Now we consider the cases where the mixture is additive but the wall treats differently both species. The extra repulsion affects the big spheres in system D and the small spheres in system E. In both cases  $\tilde{\tau}_i \leq \frac{1}{2}\sigma_i + w_i$ , so that again the correction term in Eq. (3.25) does not apply.

The results for systems D and E are shown in Figs. 5 and 6, respectively. In the case of system D there is much more room for the small spheres to sit between the wall and the big spheres than in the case of system E. As a consequence, the big spheres “feel” the presence of the wall more in the latter case than in the former and,

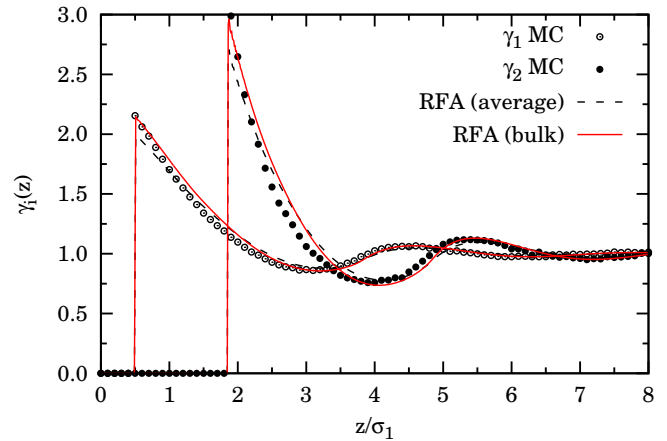


FIG. 5. (Color online) Local density profiles  $\gamma_i(z) = \rho_i(z)/\rho_i^b$  for system D ( $\sigma_2/\sigma_1 = 3$ ,  $\Delta_{12} = 0$ ,  $w_1 = 0$ ,  $w_2/\sigma_1 = 0.35$ ,  $\bar{x}_1 = 0.5$ ,  $\bar{\rho}\sigma_1^3 = 1/30$ ). The lines represent the RFA theoretical predictions using the average values  $\bar{x}_1$  and  $\bar{\rho}$  (dashed lines) or the empirical bulk values  $x_1^b$  and  $\rho^b$  (solid lines). The symbols represent our MC simulations with  $L_z/\sigma_1 = 30$ . In the MC results, the error bars are within the size of the symbols used in the graph.

thus, the contact value and the oscillations are more pronounced in system E. These effects are enhanced by the larger density of system E relative to that of system D. However,  $\gamma_1(z)$  near contact is higher in system D than in system E, so that the effect of wall nonadditivity compensates for the increase of density in the case of the small spheres, analogously to what happens with systems A and B (see Figs. 1 and 3). All these features are correctly accounted for by the RFA, although the quantitative agreement near contact is again worse than that after the first minimum, especially in the case of  $\gamma_2(z)$ . Note also that the influence on the RFA curves of the use of the bulk versus the average values is noticeable in system D but not in system E.

#### E. Nonadditive mixture and nonadditive wall

The more general situations where both the particle-particle and the wall-particle interactions are nonadditive is, of course, richer than the preceding classes. As a simple representative system we consider the same case as in system D (wall additionally repelling the big spheres), except that, in addition, species 1 and 2 interact with negative nonadditivity. The resulting system F (see Table I) is also close to system B, except that now the wall is nonadditive and the density is smaller. As in systems B–E, the correction term in Eq. (3.25) is not needed.

The local densities for system F are plotted in Fig. 7. Comparison with Fig. 5 shows that the density profile of the big spheres is practically unaffected by the

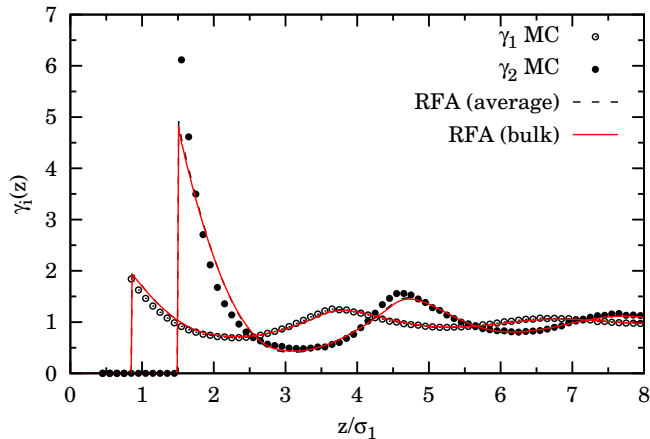


FIG. 6. (Color online) Local density profiles  $\gamma_i(z) = \rho_i(z)/\rho_i^b$  for system E ( $\sigma_2/\sigma_1 = 3$ ,  $\Delta_{12} = 0$ ,  $w_1/\sigma_1 = 0.35$ ,  $w_2 = 0$ ,  $\bar{x}_1 = 0.5$ ,  $\bar{\rho}\sigma_1^3 = 1/20$ ). The lines represent the RFA theoretical predictions using the average values  $\bar{x}_1$  and  $\bar{\rho}$  (dashed lines) or the empirical bulk values  $x_1^b$  and  $\rho^b$  (solid lines). The symbols represent our MC simulations with  $L_z/\sigma_1 = 30$ . In the MC results, the error bars are within the size of the symbols used in the graph.

nonadditive character of the 1-2 interaction. This is not surprising taking into account that, as said before, the big spheres occupy 27 times more volume than the small ones and, therefore, the presence of the latter has little impact on the properties of the former. On the contrary, the nonadditivity has a large influence on the local density profile  $\gamma_1(z)$ . Since spheres of species 1 and 2 can overlap to a certain degree in system F, the big spheres partially alleviate the influence of the wall on the small spheres with respect to the case of system D. As a consequence, the local density of the small spheres is less structured in system F than in system D. Like in system D, the RFA performs very well in system F, especially when the bulk values are used.

## VI. CONCLUSIONS

In this work we have developed a simple analytical (in Laplace space) nonperturbative theory for the local density profiles of a multicomponent fluid of NAHS confined by an additive or nonadditive hard wall. The theoretical approach is based on the specialization of the RFA technique recently proposed [28] to the case where an extra single particle of diameter  $\sigma_0$  is added to the mixture and then the limit of an infinite diameter  $\sigma_0 \rightarrow \infty$  is taken. The RFA reduces to the exact solution of the PY approximation for zero nonadditivity, both in the particle-particle and in the particle-wall interactions, but remains analytical even when nonadditivity prevents one from obtaining an analytical solution of the PY theory.

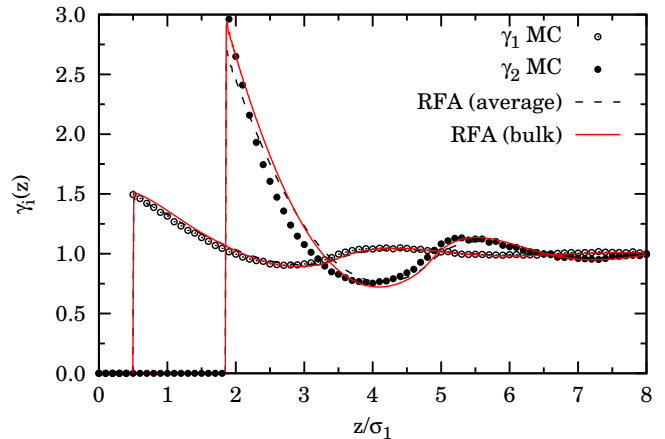


FIG. 7. (Color online) Local density profiles  $\gamma_i(z) = \rho_i(z)/\rho_i^b$  for system F ( $\sigma_2/\sigma_1 = 3$ ,  $\Delta_{12} = -0.2$ ,  $w_1 = 0$ ,  $w_2/\sigma_1 = 0.35$ ,  $\bar{x}_1 = 0.5$ ,  $\bar{\rho}\sigma_1^3 = 1/30$ ). The lines represent the RFA theoretical predictions using the average values  $\bar{x}_1$  and  $\bar{\rho}$  (dashed lines) or the empirical bulk values  $x_1^b$  and  $\rho^b$  (solid lines). The symbols represent our MC simulations with  $L_z/\sigma_1 = 30$ . In the MC results, the error bars are within the size of the symbols used in the graph.

While the theory applies to any number of components, we have focused on a binary mixture with a size ratio 1 : 3 plus a hard wall. This has allowed us to compare the theoretical results against exact MC simulation. Several representative scenarios have been considered (see Table I): a positive (system A) or negative (systems B, C1, and C2) NAHS fluid with an additive wall, an AHS mixture with a nonadditive wall pushing either the big (system D) or the small (system E) spheres, and a NAHS mixture with a nonadditive wall (system F). In all the cases, a reasonably good agreement between our theory and the MC simulations have been found for the (relative) partial local densities  $\gamma_i(z)$ . The agreement is worse near contact, where the RFA underestimates the MC values, but rapidly tends to improve for larger distances, so that the initial decay of the local densities and the subsequent oscillations are rather well captured. Note that, since the RFA can be seen as a sort of continuation of the AHS PY solution to the NAHS realm [28], it is not surprising that some of the features of the PY solution remain. One of those features is the underestimation of the contact values [13]. Another PY feature, namely the possibility of predicting a negative first minimum at sufficiently high densities, is also inherited by the RFA.

As shown by Figs. 1 and 3–7, the performance of the RFA is usually better in the case of the small spheres ( $i = 1$ ) than for the large spheres ( $i = 2$ ). This is in part due to the physical observation that the local density structure of species 1 is milder than that of species 2. Another technical reason has to do with the fact that, while the separation between both walls is sufficiently

large for the spheres near a wall not to be much influenced by the presence of the other wall, the unavoidable “compression” effect is more important for the big spheres ( $L_z/\sigma_2 = 10$ ) than for the small spheres ( $L_z/\sigma_1 = 30$ ). As Fig. 2 illustrates, when the separation between both walls is doubled, the effect on the density near the walls is more pronounced for the big spheres than for the small ones. Finite-size effects are also related to the small differences between the *average* densities and their *bulk* values in the central region  $z \approx L_z/2$ . We have checked that our theoretical approach exhibits a slightly better agreement with simulations when the empirical bulk values are used instead of the average values.

Our theory, being a simple analytical one, can be efficiently used to easily extract many-body approximate properties for confined fluids under other interesting situations different from the representative ones examined in this work. For instance, extreme cases like the Widom–Rowlinson [44–46] ( $\sigma_1 = \sigma_2 = 0$  with  $\sigma_{12}$  finite) or the Asakura–Oosawa [47, 48] ( $\sigma_1 = 0$  and  $\Delta_{12} > 0$ ) confined fluids can be studied. Another avenue for application of the RFA is the depletion potential between two big spheres immersed in a sea of small spheres [49] interacting nonadditively with them.

### Appendix: Evaluation of $\tilde{L}_i(s)$ and $\tilde{A}_j(s)$

Let us recall that  $\sigma_{i0} = \frac{1}{2}(\sigma_i + \sigma_0) + w_i$  with  $w_i \geq 0$ . Therefore, according to Eq. (3.6),  $b_{i0} = \sigma_i + w_i$ . Thus, Eqs. (3.10)–(3.12) yield

$$\Lambda_0 = \frac{\sigma_0}{2}M_{2,0} + \frac{1}{6}M_{3,0} + \frac{1}{2}M_{2,1}, \quad (\text{A.1})$$

$$\Psi_0 = -\frac{\sigma_0}{2}M_{2,0} + \frac{1}{6}M_{3,0} - \frac{1}{2}M_{2,1}, \quad (\text{A.2})$$

$$\Omega_0 = -\frac{\sigma_0^2}{4}M_{2,0} - \frac{\sigma_0}{2}M_{2,1} - \frac{1}{4}M_{2,2}, \quad (\text{A.3})$$

where

$$M_{p,q} \equiv \sum_{k=1}^n \bar{x}_k (\sigma_k + w_k)^p w_k^q, \quad q \geq 0. \quad (\text{A.4})$$

Interestingly enough, the terms proportional to  $\sigma_0$  and to  $\sigma_0^2$  in the denominator of Eqs. (3.8) and (3.9) cancel,

so that the denominator becomes

$$\tilde{D} \equiv \left(1 - \frac{\pi}{6}\bar{\rho}M_{3,0}\right)^2 - \frac{\pi^2}{4}\bar{\rho}^2(M_{2,1}^2 - M_{2,0}M_{2,2}). \quad (\text{A.5})$$

Equations (A.1)–(A.5) apply to any value of  $\sigma_0$ . From Eqs. (3.7)–(3.9) it is easy to see that both  $L_{i0}^{(0)}$  and  $L_{i0}^{(1)}$  are linear functions of  $\sigma_0$ . Thus, taking the limit (3.23) one gets

$$\tilde{L}_i(s) = \tilde{L}^{(0)} + \tilde{L}_i^{(1)}s \quad (\text{A.6})$$

with

$$\tilde{L}^{(0)} = \frac{\pi\bar{\rho}M_{2,0}}{2\tilde{D}}, \quad (\text{A.7})$$

$$\tilde{L}_i^{(1)} = \frac{1}{2\tilde{D}} \left[1 - \frac{\pi}{6}\bar{\rho}(M_{3,0} + 3M_{2,1}) + \left(\frac{\sigma_i}{2} + w_i\right)\pi\bar{\rho}M_{2,0}\right]. \quad (\text{A.8})$$

Analogously, from Eqs. (3.3) and (3.5), the limit (3.24) becomes

$$\tilde{A}_j(s) = \frac{2\pi\bar{\rho}\bar{x}_j}{s^3} e^{\sigma_j s/2} \left[\tilde{N}_j(s) - \tilde{L}_j(s)e^{-(\sigma_j + w_j)s}\right], \quad (\text{A.9})$$

where

$$\begin{aligned} \tilde{N}_j(s) = \tilde{L}^{(0)} & \left[1 - (\sigma_j + w_j)s + \frac{(\sigma_j + w_j)^2 s^2}{2}\right] \\ & + \tilde{L}_j^{(1)}s [1 - (\sigma_j + w_j)s]. \end{aligned} \quad (\text{A.10})$$

### ACKNOWLEDGMENTS

The authors are grateful to the referees for suggestions contributing to the improvement of the paper. R.F. would like to acknowledge the use of the computational facilities of CINECA through the ISCR call. A.S. acknowledges support from the Ministerio de Ciencia e Innovación (Spain) through Grant No. FIS2010-16587 and the Junta de Extremadura (Spain) through Grant No. GR10158, partially financed by Fondo Europeo de Desarrollo Regional (FEDER) funds.

- 
- [1] D. Henderson, F. F. Abraham, and J. A. Barker, *Mol. Phys.* **31**, 1291 (1976).  
 [2] D. Henderson, *J. Chem. Phys.* **68**, 780 (1978).  
 [3] M. Plischke and D. Henderson, *J. Phys. Chem.* **88**, 6544 (1984).  
 [4] M. Plischke and D. Henderson, *J. Chem. Phys.* **84**, 2846

- (1985).  
 [5] D. Henderson, K.-Y. Chan, and L. Degréve, *J. Chem. Phys.* **101**, 6975 (1994).  
 [6] R. Dickman, P. Attard, and V. Simonian, *J. Chem. Phys.* **107**, 205 (1997).  
 [7] W. Olivares-Rivas, L. Degréve, D. Henderson, and J.

- Quintana, J. Chem. Phys. **106**, 8160 (1997).
- [8] J. Noworyta, D. Henderson, S. Sokolowski, and J.-Y. Chan, Mol. Phys. **95**, 415 (1998).
- [9] Z. Tan, U. Marini Bettolo Marconi, F. van Swol, and K. E. Gubbins, J. Chem. Phys. **90**, 3704 (1989).
- [10] I. K. Snook and D. Henderson, J. Chem. Phys. **68**, 2134 (1978).
- [11] L. Degréve and D. Henderson, J. Chem. Phys. **100**, 1606 (1993).
- [12] M. Rottereau, T. Nicolai, and J. C. Gimel, Eur. Phys. J. E **18**, 37 (2005).
- [13] A. Malijevský, S. B. Yuste, A. Santos, and M. López de Haro, Phys. Rev. E **75**, 061201 (2007).
- [14] C. N. Patra and S. K. Ghosh, J. Chem. Phys. **106**, 2762 (1997).
- [15] C. N. Patra, J. Chem. Phys. **111**, 6573 (1999).
- [16] R. Roth and S. Dietrich, Phys. Rev. E **62**, 6926 (2000).
- [17] S. Zhou and E. Ruckenstein, J. Chem. Phys. **112**, 5242 (2000).
- [18] S. Zhou, Phys. Rev. E **63**, 061206 (2001).
- [19] N. Choudhury and S. K. Ghosh, J. Chem. Phys. **114**, 8530 (2001).
- [20] C. N. Patra and S. K. Ghosh, J. Chem. Phys. **116**, 8509 (2002).
- [21] C. N. Patra and S. K. Ghosh, J. Chem. Phys. **116**, 9845 (2002).
- [22] C. N. Patra and S. K. Ghosh, J. Chem. Phys. **117**, 8933 (2002).
- [23] C. N. Patra and S. K. Ghosh, J. Chem. Phys. **118**, 3668 (2003).
- [24] Y. Duda, E. Vakarin, and J. Alejandre, J. Colloid Interf. Sci. **258**, 10 (2003).
- [25] A. Patrykiewicz, S. Sokolowski, and O. Pizio, J. Phys. Chem. B **109**, 14227 (2005).
- [26] F. Jiménez-Ángeles, Y. Duda, G. Odriozola, and M. Lozada-Cassou, J. Phys. Chem. C **112**, 18028 (2008).
- [27] P. Hopkins and M. Schmidt, Phys. Rev. E **83**, 050602 (2011).
- [28] R. Fantoni and A. Santos, Phys. Rev. E **84**, 041201 (2011), Note that in Eq. (2.12) the hats on the partial correlation functions should be replaced by tildes.
- [29] S. B. Yuste, M. López de Haro, and A. Santos, Phys. Rev. E **53**, 4820 (1996).
- [30] M. López de Haro, S. B. Yuste, and A. Santos, in *Theory and Simulation of Hard-Sphere Fluids and Related Systems*, edited by A. Mulero (Springer-Verlag, Berlin, 2008), vol. 753 of *Lectures Notes in Physics*, pp. 183–245.
- [31] J.-P. Hansen and I. R. McDonald, *Theory of Simple Liquids* (Academic Press, London, 2006).
- [32] R. Fantoni and G. Pastore, J. Chem. Phys. **119**, 3810 (2003).
- [33] A. González, J. A. White, F. L. Román, and S. Velasco, J. Chem. Phys. **135**, 154704 (2011).
- [34] Z. W. Salsburg, R. W. Zwanzig, and J. G. Kirkwood, J. Chem. Phys. **21**, 1098 (1953).
- [35] J. L. Lebowitz and D. Zomick, J. Chem. Phys. **54**, 3335 (1971).
- [36] M. Heying and D. S. Corti, Fluid Phase Equil. **220**, 85 (2004).
- [37] A. Santos, Phys. Rev. E **76**, 062201 (2007).
- [38] J. L. Lebowitz, Phys. Rev. **133**, A895 (1964).
- [39] S. B. Yuste, A. Santos, and M. López de Haro, J. Chem. Phys. **108**, 3683 (1998).
- [40] R. D. Rohrmann and A. Santos, Phys. Rev. E **83**, 011201 (2011).
- [41] R. D. Rohrmann and A. Santos, Phys. Rev. E **84**, 041203 (2011).
- [42] J. Abate and W. Whitt, Queueing Systems **10**, 5 (1992).
- [43] D. Henderson and P. J. Leonard, Proc. Natl. Acad. Sci. USA **67**, 1818 (1970).
- [44] B. Widom and J. Rowlinson, J. Chem. Phys. **15**, 1670 (1970).
- [45] D. Ruelle, Phys. Rev. Lett. **16**, 1040 (1971).
- [46] R. Fantoni and G. Pastore, Physics A **332**, 349 (2004), Note that there is a misprint in Eq. (13), which should read  $\tilde{h}_{12}(k) = \tilde{c}_{12}(k)[1 - \rho_1\rho_2\tilde{c}_{12}^2(k)]^{-1}$ .
- [47] S. Asakura and F. Oosawa, J. Chem. Phys. **22**, 1255 (1954).
- [48] S. Asakura and F. Oosawa, J. Polym. Sci. **33**, 183 (1958).
- [49] S. B. Yuste, A. Santos, and M. López de Haro, J. Chem. Phys. **128**, 134507 (2008).